AN ANALYSIS OF CARCASS LAYER EROSION IN UN-BONDED FLEXIBLE OFFSHORE PIPEWORK

(DOI No: 10.3940/rina.ijme.2021.a1.640)

C An, **C W Gu**, **H Qin**, College of Safety and Ocean Engineering, China University of Petroleum-Beijing, China, **T T Li***, National Science Library, Chinese Academy of Sciences, China, **M L Duan**, College of Safety and Ocean Engineering, China University of Petroleum-Beijing, China
* Correspondence: litongtong@mail.las.ac.cn

KEY DATES: Submitted: 23/04/2020, Final acceptance: 22/01/2021, Published: 25/03/2021

SUMMARY

In this paper, a simplified model for erosion in un-bonded flexible pipes caused by the sand entrained in the produced fluid is established. Flow field analysis is performed based on the governing equations of the continuous fluid and the discrete particles. A two-way coupled Eulerian-Lagrangian approach is employed to solve the gas-solid flow in the pipe bend. To eliminate the influence of the length of the straight pipe section on the stability of the flow field in the pipe, the flow field distribution under different lengths is analyzed to determine the optimal straight pipe length. Six commonly used erosion models are adopted to predict the erosion rate. After comparing the prediction results with experimental data, the most accurate Oka model is selected to calculate the effect of the fluid and structure parameters on erosion. Effects of particle parameters and pipe structural parameters on the erosion rate of curved flexible pipes are numerically fitted, and the quantitative description is given.

NOMENCLATURE

BH	*Brinell hardness of pipe wall material*
$C_{1\varepsilon}$	*Constant taken as 1.44*
$C_{2\varepsilon}$	*Constant taken as 1.92*
C_μ	*Constant taken as 0.09*
C_D	*Drag coefficient*
D	*Flexible pipe diameter*
d'	*Reference erosion depth*
d_p	*Particle diameter*
ED	*Erosion depth*
EL	*Mass loss*
EW	*Maximum erosion depth*
F_s	*Shape coefficient of particles*
f_i	*Unit mass force*
$f(\alpha)$	*Impact angle function*
g	*Acceleration of gravity*
Hv	*Dimensional hardness*
k	*Turbulent kinetic energy*
MR	*Mass flow rate*
p	*Pressure of the fluid*
R	*Flexible pipe curvature*
Re	*Relative Reynolds number*
S_i	*Momentum transfer between continuous and discrete phases*
t	*Time duration the flexible pipe is impacted*
u_i	*Velocity components of the fluid*
u_p	*Particle velocity*
v'	*Reference erosion velocity*
α	*Impact angle*
α_0	*Maximum erosion angle*
ε	*Turbulent dissipation rate*
μ	*Dynamic viscosity of the fluid*
μ_t	*Turbulent viscosity*
ρ	*Gas density*
ρ_p	*Particle density*

1. INTRODUCTION

Un-bonded flexible pipes are widely used in the field of offshore oil and gas engineering. The bearing conditions of flexible pipes are complex, such as large tensile loads, cyclic loads, external pressure, internal fluid pressure, coupled axial compression and bending loads. Different layers of un-bonded flexible pipes have different functions (PSA-Norway, 2007) and the skeleton layer is in direct contact with the production fluid inside the flowline system. If the transport medium contains sand particles, the skeleton layer will face the potential risks of erosion and wear, which may lead to reduced load resistance or even the internal fluid leakage. Although there are many achievements on the limit strength of carcass layer of flexible pipe under external pressure (Niels *et al*., 2012; Tang *et al*., 2016; Li *et al*., 2018), few literatures are found on the carcass erosion, which is an essential concern for the safe operation of flexible pipes.

The sand erosion behavior in oil and gas pipeline has been widely studied. Chen *et al*. (2004) verified the impact of the particle-wall rebound models on the erosion pattern of 90° elbow, and tested their models by performing some erosion tests. Arabnejad *et al*. (2015) developed a new semi-mechanical erosion equation based on the experimental data of direct impact test, which explained the characteristics of particles and target materials. Parsi *et al*. (2017a，2017b) studied the erosion of standard elbow under the action of gas-liquid-solid multiphase flow, and evaluated the computational fluid dynamics (CFD) simulation results with previous experimental data. Banakermani *et al*. (2018) studied the total erosion and maximum erosion rate of elbows with different geometric shapes from 15° to 90° within a certain mass loading range. It was found that the maximum erosion rate was approximately 55° on the elbow wall for vertical inlet-horizontal outlet (V-H) configuration and approximately 50° for horizontal inlet-horizontal outlet (H-H) configuration.

The increased use of flexible pipes in subsea requires researchers to carefully assess the risks of the rough internal surface erosion of flexible pipes formed by interlocking carcass. Kvernvold and Nokleberg (1989) found that the unevenness inside the bending flexible pipe could lead to the erosion of the pipe. During the erosion simulation of the skeleton layer of the bending flexible pipe, the unevenness inside was modeled as a triangle, and the simulation results showed that the erosion amount in the irregular part was one order of magnitude higher than that in other parts. Kvernvold *et al*. (1990) carried out erosion experiment analysis based on the previous erosion simulation of the flexible pipe, in which 250 μm of sand particles was mixed in nitrogen for transportation. It was found that the erosion rate of the skeletal layer facing the particles was high, while the erosion of the skeletal layer on the other side was almost zero. Chong *et al*. (2015) proposed an erosion formula for rough surface based on the calculation formula for the erosion rate of elbow in DNV standard. Based on the theoretical calculation of erosion rate on the simplified inner surface of the skeleton layer, and comparing with related smooth pipe erosion experiments, the error was found to be within 50%. Helgaker *et al*. (2017) carried out erosion simulation and experimental analysis on carcass skeleton layer of bending flexible pipe, where 11 groups of different experiments were carried out to measure the mass loss of carcass and the erosion depth along the contour.

The purpose of this work is to propose an appropriate model to predict the erosion distribution and erosion rate of flexible pipes under different influence factors. The characteristics of the current erosion models are presented. CFD simulations are used to predict the flow field distribution and erosion rates. Comparing with different erosion prediction models and experimental data, a simplified model of the erosion of curved flexible pipe is established.

2. MATHEMATICAL MODEL

When analyzing the erosion problem of two phase flow of fluid carrying sand, the liquid is usually regarded as a continuous phase. The Eulerian-Lagrangian method, which is commonly chosen for modeling the two-phase flow, relies on solving Navier-Stokes equations for the fluid phase as the continuous phase while the dispersed phase (solid particles) are modeled using Lagrangian tracking approach. Two-way coupling is applied between the continuous phase and discrete phase (Zamani *et al*., 2017, Parsi *et al*., 2014).

2.1 FLUID PHASE MODELING

The Navier-Stokes equations represent the conservation of momentum, while the continuity equation represents the conservation of mass:

$$\frac{\partial \rho}{\partial t}+\frac{\partial(\rho u_x)}{\partial x}+\frac{\partial(\rho u_y)}{\partial y}+\frac{\partial(\rho u_z)}{\partial z}=0 \tag{1}$$

$$\frac{\partial(\rho u_i)}{\partial t}+\frac{\partial(\rho u_i u_j)}{\partial x_j}=-\frac{\partial p}{\partial x_i}+\frac{\partial}{\partial x_j}\left(\mu\frac{\partial u_i}{\partial x_j}-\rho\overline{u_i' u_j'}\right)+\rho f_i+S_i \tag{2}$$

where u_x, u_y, u_z are the velocity components of the fluid in x, y, z directions, m/s; ρ is the density, kg/m^3; μ is the dynamic viscosity of the fluid, Pa•s; x_i represents the three directions of x, y and z, respectively; f_i represents the unit mass force in the three directions of x, y and z, N; p is pressure, Pa; S_i represents momentum transfer between continuous and discrete phases in different directions, respectively.

A standard k-ε turbulence model with a standard wall function is used to solve the flow turbulence:

Turbulent kinetic energy k:

$$\frac{\partial(\rho k)}{\partial t}+\frac{\partial(\rho k u_j)}{\partial x_i}=\frac{\partial}{\partial x_j}\left[\left(\mu+\frac{\mu_t}{\sigma_k}\right)\frac{\partial k}{\partial x_i}\right]+G_k+G_b-Y_m-\rho\varepsilon+S_k \tag{3}$$

Turbulent kinetic energy dissipation rate ε:

$$\frac{\partial(\rho\varepsilon)}{\partial t}+\frac{\partial(\rho k u_j)}{\partial x_i}=\frac{\partial}{\partial x_j}\left[\left(\mu+\frac{\mu_t}{\sigma_\varepsilon}\right)\frac{\partial k}{\partial x_i}\right]+C_{1\varepsilon}\frac{\varepsilon}{k}C_k-C_{2\varepsilon}\rho\frac{\varepsilon^2}{k}+S_\varepsilon \tag{4}$$

where, k is turbulent kinetic energy, J; μ_t is turbulent viscosity, Pa•s; σ_k = 1.0 is the Prandtl number corresponding to turbulent kinetic energy; G_k is the turbulent kinetic energy caused by the average velocity; G_b is the turbulent kinetic energy caused by the influence of buoyancy; ε is the turbulent dissipation rate, W/m^3; Y_m is the effect of turbulence pulsation on dissipation rate; σ_ε = 1.3 is the Prandtl number corresponding to the turbulent energy dissipation rate; $C_{1\varepsilon}$ = 1.44, $C_{2\varepsilon}$ = 1.92 and C_μ = 0.09, which are determined from turbulent shear flow experiments; S_k and S_ε are user-defined source terms.(Versteeg and Malalasekera, 2007)

2.2 PARTICLE PHASE MODELING

The motion of the particles in the discrete phase in the fluid is determined by Newton's second law. The equation of motion of the particles in the Lagrange coordinate system can be expressed as follows:

$$\frac{du_p}{dt}=F_D(u-u_p)+F_P+F_{VM}+F_G \tag{5}$$

From the first term to the fourth term on the right side of the equation are: drag force, pressure gradient force, additional mass force and buoyancy force. $F_D(u-u_p)$ is the drag force per unit mass, *N*, which can be expressed by

$$F_D=\frac{18\mu}{\rho_p d_p^2}\frac{C_D Re}{24} \tag{6}$$

where *u* is the fluid velocity, m/s; u_p is the particle velocity, m/s; ρ_p is the density of particles, kg/m^3, d_p is the diameter of particles, m; C_D is the drag coefficient. *Re* is the relative Reynolds number:

$$Re=\frac{\rho d_p|u-u_p|}{\mu} \tag{7}$$

C_D is the coefficient of drag force:

$$C_D=\alpha_1+\frac{\alpha_2}{Re}+\frac{\alpha_3}{Re^2} \tag{8}$$

where α_1, α_2, α_3 are constants for the smooth spherical particles. Morsi and Alexander (1972) gave different values of α_1, α_2, α_3 for different Reynolds numbers.

When there is a pressure gradient in the flow field, the pressure gradient force on a single particle in the flow field is:

$$F_p=-V_p\frac{\partial p}{\partial x} \tag{9}$$

The additional mass force, F_{vm}, can be generated from the motion of the surrounding fluid driven by the discrete phase movement. It is expressed as:

$$F_{vm}=\frac{1}{2}\rho V_p\left(\frac{du}{dt}-\frac{du_t}{dt}\right) \tag{10}$$

The formula of buoyancy is:

$$\overrightarrow{F_G}=\frac{(\rho_P-\rho)}{\rho_P}\vec{g} \tag{11}$$

Where ρ is the density of fluid, kg/m^3, ρ_p is the density of particles, kg/m^3.

2.3 EROSION MODELS

The current typical particle erosion models include: the Finnie classic wear model, the E/CRC erosion model, the DNV erosion model, the Oka erosion model, the Ahlert model and the Tabakoff erosion model, which are described below.

2.3 (a) Finnie model

Finnie (1958) established a theoretical model of particle erosion, highlighting the impact of particle velocity and incidence angle.

$$ER=kv^n f(\alpha) \tag{12}$$

$$f(\alpha)=\begin{cases} \sin(2\alpha)-3\sin(\alpha) & \alpha\le\alpha_0 \\ \cos^2\alpha/3 & \alpha>\alpha_0 \end{cases} \tag{13}$$

where *k* is a proportional constant; *n* is an empirical coefficient, which are 2 to 4 for brittle materials, and 1.8-2.3 for plastic materials; α is the impact angle, rad; $f(\alpha)$ is the impact angle function; α_0 is the maximum erosion angle, which is usually taken as 15.3°.

2.3 (b) E/CRC model

The E/CRC model was proposed by the Erosion / Corrosion Research Center of Tulsa University based on the Finnie model using LDV (Laser Doppler Velocimeter). The model is as follows (Zhang *et al.*, 2007):

$$ER=C(BH)^{-0.59}F_s v^n f(\alpha) \tag{14}$$

$$f(\alpha)=5.40\alpha-10.11\alpha^2+10.93\alpha^3-6.33\alpha^4+1.42\alpha^5 \tag{15}$$

where, *C* represents a constant; *n* represents the velocity index, which is 2.41; *BH* represents Brinell hardness of pipe wall material, MPa; F_s represents the shape coefficient of particles, 1.0 for sharp particles, 0.2 for completely spherical particles, and 0.53 for those in between; *v* represents the velocity at which particles hit the material, m/s; *n* is the empirical coefficient; α is the angle at which the particles hit the tube wall; $f(\alpha)$ represents the impact angle function fitted by experimental data.

2.3 (c) Ahlert model

Ahlert (1994) proposed the erosion model as:

$$ER=1.559e^{-6}BH^{-0.59}F_s v^n f(\alpha) \tag{16}$$

$$f(\alpha)=\begin{cases} 2.27\alpha-3.84\alpha^2 & \alpha\le\alpha_0 \\ 3.147\cos^2\alpha\sin\alpha+0.3609\sin^2\alpha+2.532 & \alpha>\alpha_0 \end{cases} \tag{17}$$

where, *BH* represents the Brinell hardness of the pipe wall material, MPa; F_s is the shape coefficient of particles, which is 1.0 for polygonal particles, 0.53 for semicircular particles, and 0.2 for completely circular particles; *v* represents the velocity at which particles hit the material, m/s; *n* is the empirical coefficient; α is the angle at which the particles hit the tube wall; $f(\alpha)$ represents the impact angle function fitted by experimental data; α_0 is the maximum erosion angle, which is usually taken as 15.3°.

2.3 (d) Oka model

The Oka model (Oka and Okamura, 2005; Oka and Yoshida, 2005) is as follows:

$$ER=C\rho f(\alpha)(H_v)^{k_1}\left(\frac{v}{v'}\right)^{k_2}\left(\frac{d}{d'}\right)^{k_3} \tag{18}$$

$$f(\alpha)=(sin\alpha)^{n_1}[1+H_v(1-sin\alpha)]^{n_2} \tag{19}$$

where, C is a constant, which is 10^{-9}; ρ is the density of the analyzed component kg/m^3; Hv is the dimensional hardness of the analyzed component, MPa; v' is the reference erosion velocity, m/s; d' is the reference erosion depth, m; k_1, k_2, k_3, n_1 and n_2 are constants.

2.3 (e) DNV model

Det Norske Veritas (2007) obtained the following corrosion prediction model based on their experimental data. The erosion rate at the elbow can be calculated by:

$$ER=Cf(\alpha)v^{n} \tag{20}$$

$$f(\alpha)=\sum_{i=1}^{8}(-1)^{i+1}A_i\,\alpha^{i} \tag{21}$$

where, $C = 2^{-9}$ is a constant; $n = 2.6$ is the speed index; A_1, A_2, and A_3 are constants.

2.3 (f) Tabakoff model

Grant and Tabakoff (1973) developed a semi-empirical relationship to predict erosion rates with different particle velocities and impact angles. The model is as follows:

$$ER=f(\alpha)\left(\frac{v}{V_1}\right)^2 cos^2\alpha\left[1-\left(1-\frac{v}{V_3}sin\alpha\right)^2+\left(\frac{v}{V_2}sin\alpha\right)^4\right] \tag{22}$$

$$f(\alpha)=\left[1+k_1k_2sin\left(\alpha\frac{\pi}{2\alpha_0}\right)\right]^2 \tag{23}$$

$$k_1=\begin{cases}1.0 & \alpha\leq2\alpha_0\\ 0.0 & \alpha>2\alpha_0\end{cases} \tag{24}$$

where, k_1, k_2 and θ_0 are constants, v represents the velocity at which particles hit the material, m/s; V_1, V_2 and V_3 are relevant parameters of erosion velocity.

The Lagrangian method is used to track the particles to obtain the momentum change, which is applied to the subsequent calculation of the continuous phase flow field, and the continuous phase is solved simultaneously in the process of solving the particle trajectory. The coupling is achieved by alternately solving the continuous phase and discrete phase governing equations until convergence is achieved. The relationship between the speed and the collision angle after the collision is obtained through the wall collision recovery coefficient, and the erosion rate under different conditions is obtained through the subsequent erosion prediction model introduced.

3. CFD MODELING

3.1 PROBLEM DESCRIPTION

The simulation results obtained using the ANSYS FLUENT CFD software are verified with the experimental results conducted by DNV GL. Helgaker *et al.* (2017) carried out 11 sets of quartz sand erosion experiments for flexible pipes. In the experiment, the particle velocity is 30 m/s~47 m/s, and the particle size is 150 μm~550 μm. The experimental conditions are shown in the Table 1. The test result from Helgker et al. (2017) is expressed in mm/ton, where mm is the depth of the erosion location, and ton is the weight of the sand. However, the unit of the result of the simulation is ER (kg/m^2•s), therefore the researches introduce the material density ρ (kg/m^3), the duration of time that the flexible pipe undertakes erosion t (s), the mass flow rate MR (kg/s), the total mass of sand M (kg), in order to compare the results between the test and the simulation in the same unit system. The unit of the maximum erosion depth EW is m/kg, which represents the maximum erosion depth caused by a unit mass of sand. The unit of erosion depth ED is m/s, which represents the depth of sand erosion per unit time. The mass loss *EL* (kg) can describe the mass loss of the component within a certain time. The conversion relationship is as follows:

$$ED=\frac{ER}{\rho} \tag{25}$$

$$EL=ER\cdot A\cdot t \tag{26}$$

$$EW=\frac{ED}{MR}=\frac{ER}{\rho\bullet MR} \tag{27}$$

where, ρ represents the density of the flexible pipe (kg/m^3); A represents the surface area of the flexible pipe subjected to impact erosion (m^2); t represents the time duration that the flexible pipe is impacted, s; MR is mass flow rate, kg/s.

Table 1 Helgaker erosion test condition

Working condition	Particle velocity (*m/s*)	Particle diameter (*μm)*	Mass flow rate (*g/s*)	Sand quality (*kg)*	Pipe curvature (*r/D)*
1	47	150	100	1000	10
2	36	150	100	300	10
3	30	550	100	200	10
4	30	150	100	300	10
5	30	250	100	300	10
6	35	550	100	300	10
7	35	250	100	300	10
8	35	150	100	1500	10
9	40	550	100	300	10
10	40	250	100	300	10
11	40	150	100	300	10

3.2 SIMPLIFIED GEOMETRY OF CARCASS LAYER

The flexible pipe composite structure combines steel armor layers with high stiffness to provide strength and polymer sealing layers with low stiffness to provide fluid integrity. The present work only concerns the inner layer viz., carcass, of the flexible pipe, where the erosion phenomenon takes place. Considering the complicated groove structure as shown in Figure 1, it is difficult to implement the mesh of the slits (in the red circle) formed at the contact interface between different carcass contours (such as the inner contour of carcass2 and the outer contour of carcass3). Since the direction of internal fluid flow is from left to right, only a small part of the groove can collide with the solid particles. Meanwhile, Helgaker's experiments showed that erosion was mainly distributed at the arcs (the green color line and the blue rectangle in Figure 1), however, there was almost no erosion at the slit. Therefore, the inter-lock structure of carcass in Figure 1 can be simplified to the structure described in Figure 2. This article mainly focuses on whether the erosion of the pipe wall caused by the sand-carrying fluid will cause the penetration of the carcass layer, so the analysis object in this paper is the fluid domain enclosed by the carcass. The geometric parameters and physical properties of the simplified un-bonded flexible pipe are given in Table 2, and the simplified model of un-bonded flexible pipes is shown in Figure 3.

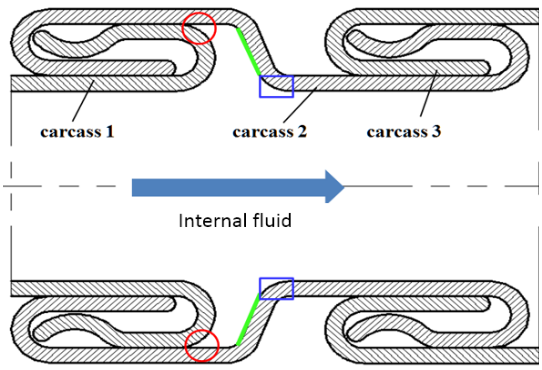

Figure 1 Real inter-lock structure diagram of carcass

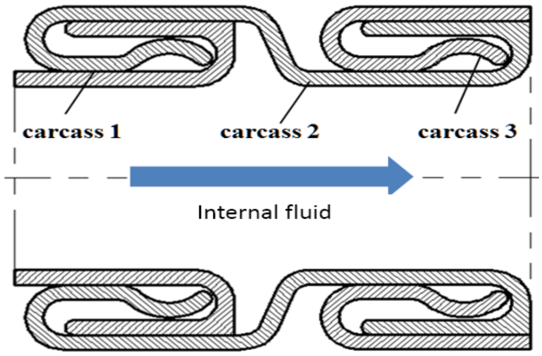

Figure 2 Simplified inter-lock structure diagram of carcass

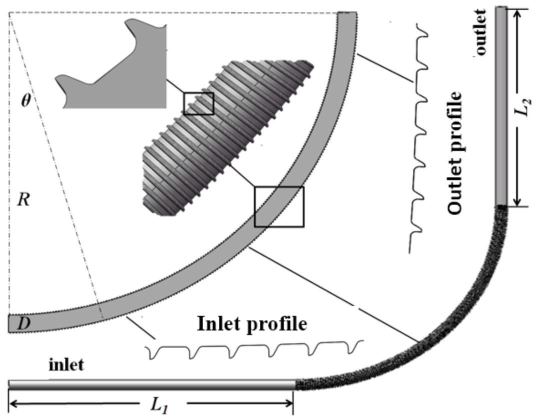

Figure 3 Simplification of fluid domain inside unbonded flexible pipe

3.3 MESHING

After the model of the fluid domain inside the flexible pipe is established, in order to generate fully developed turbulence flow and eliminate the influence of outlet reverse flow on the fluid pattern in the flexible pipe, each straight pipe section needs to be added at the inlet and outlet of the flexible pipe, respectively, as shown in Figure 3. The appropriate length L_1 of straight pipe at the inlet and length L_2 of straight pipe at the outlet should be determined by performing the sensitivity analysis. The inlet particle velocity is 20 m/s, the particle mass flow rate is 0.01 kg/s, and the particle diameter is 200 μm.

Table 2 Basic parameters of un-bonded flexible pipes model

Parameter	**Unit**	**Description**
Flexible pipe diameter D	*in*	4
Flexible pipe curvature R	*in*	72
Pipe material	/	Carbon steel
material density ρ_f	kg/m^3	7860
Hardness BH	/	160
Internal fluid	/	Natural gas
Gas density ρ	kg/m^3	0.6679
Sand type	/	Quartz sand
Particle density ρ_p	kg/m^3	2650
g	m/s^2	-9.8

Table 3 Erosion rate prediction of the carcass with different lengths of straight pipes

Length of straight pipe L_1	4D	8D	12D	16D	20D
Length of straight pipe L_2	2D	4D	6D	8D	10D
Number of grids	4105759	4797223	5437767	6101435	6782994
Relative error for grids	39.46%	29.28%	19.83%	10.04%	—
Maximum erosion rate (kg/m^2·s)	5.71e-6	5.56e-6	5.27e-6	5.34e-6	5.40e-6
Relative error for maximum erosion rate	5.74%	2.96%	2.41%	1.11%	—

The results for erosion rate prediction of the steel carcass with different length of straight pipes at the inlet and outlet are shown as Table 3. The results of (a) L_1 = 16D, L_2 = 8D, (b) L_1 = 12D, L_2 = 6D, (c) L_1 = 8D, L_2 = 4D and (d) L_1 = 4D, L_2 = 2D are compared with the one of 20D (10D), respectively. The calculation results show that as the length of L1 and L2 increases, the result of erosion fluctuates up and down, and eventually stabilizes. The longer L1 and L2, the better, but the main object of the calculation in this paper is the curved section, and considering the calculation cost, it is not possible to choose a straight pipe section that is too long. To effectively reduce the calculation amount and ensure the simulation accuracy, the lengths of L_1 = 8D and L_2 = 4D are selected for the straight sections of inlet and outlet pipes section.

There are many grooves on the inner surface of carcass, therefore it is impossible to divide the mesh by sweeping method, but only to employ refined tetrahedral mesh to improve the calculation accuracy. The sweep method for hexahedral meshing is used in the straight pipe segment at the inlet and outlet. The wall boundary layer is set with 12 layers with a growth rate of 1.2 for smooth transition between fine mesh near the wall to coarse cell around. The CFD mesh of internal flow inside the carcass layer of the flexible pipe is generated as shown in Figure 4.

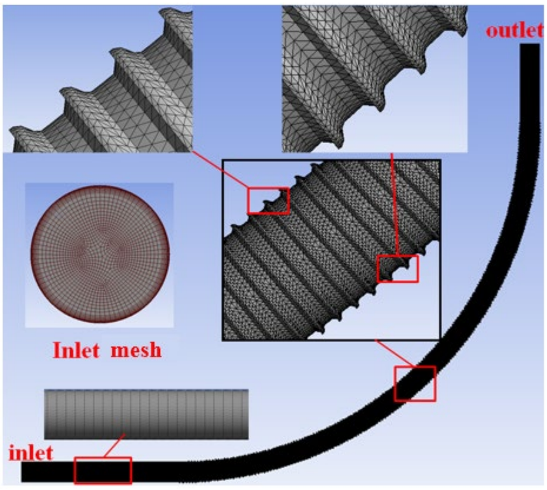

Figure 4 CFD Mesh of internal flow in un-bonded flexible pipes

Table 4 Erosion rate prediction of the carcass with different mesh densities

Grid size	Number of nodes	Number of grids	Maximum erosion rate kg/m^2·s	Relative error
8 mm	155622	736017	5.65e-6	5.81%
7 mm	206341	1033138	5.84e-6	9.36%
6 mm	296375	1515649	5.66e-6	5.99%
5 mm	489699	2596068	5.49e-6	2.81%
4 mm	872651	4797223	5.36e-6	0.37%
3 mm	1956152	11077263	5.34e-6	—

The appropriate mesh density should be also determined. For inlet particle velocity of 20 m/s, particle mass flow of 0.01 kg/s, particle diameter of 200 μm, inlet straight pipe section $L_1 = 8D$, outlet straight pipe section length L2 = 4D. The result for erosion rate prediction of the carcass with different mesh densities, viz., 3~8 mm is shown as Table 4. The results for erosion rates are calculated with the grid sizes of 4 mm, 5 mm, 6 mm, 7 mm and 8 mm, and compared with the one obtained with the grid size of 3 mm, respectively. As provided in Table 4, when the mesh size changes from 3 mm to 4 mm, the maximum erosion rate changes from 5.34e-6 kg/m^2•s to 5.36e-6 kg/m^2•s, with a relative error of 0.37%. Therefore, the mesh with the size of 4 mm is used to discrete the fluid field in this work.

4. RESULTS AND DISCUSSION

4.1 SELECTION OF EROSION MODEL

As discussed in Section 2.3, the different corrosive materials, objects being eroded and particle characteristics in experiments determine different erosion prediction models obtained. Therefore, the prediction models based on experimental data have certain limitations. The E/CRC model (Zhang *et al*., 2007) is an erosion model obtained with quarts as the corrosive material and carbon steel as the object being eroded. The Oka model (Oka and Okamura, 2005; Oka and Yoshida, 2005) is applicable to the prediction of erosion when corrosive materials such as quartz sand and glass beads are used to erode materials such as stainless steel and carbon steel. The DNV model (2007) is suitable for the erosion prediction of materials such as steel, aluminum, high alloy steel, etc., as the objects being eroded. The particles used in Tabakoff model (Grant and Tabakoff, 1973) are pulverized coal. And he Ahlert model (Ahlert, 1994) is established based on the experiment with quartz sand as the corrosive material to erode carbon steel - Q235. The object being eroded in this work is steel, and the erosion material is quartz sand. Therefore, the erosion prediction models applicable to this present work are narrowed down to E/CRC model, Ahlert model, DNV model, and Oka model.

Each erosion prediction model contains parameters that affect the erosion results, such as particle velocity, particle diameter, particle mass flow rate, etc. The most important impact parameter is the impact angle function, which defines the particle flow direction of particles after collision and directly affects the final erosion results (Wang *et al*., 2016). This paper compares the impact angle functions of the four models, and the results are summarized in Figure 5.

From the impact angle function curves of four different models, the impact angle function value of the Ahlert model is much larger than the other three models. Chen *et al*. (2004) found that using this model to predict erosion can be much larger than the experimental results, mainly because the velocity index in this model is 1.73, which is higher than the recommended value in other models. Therefore, Ahlert model is not applicable in this work to predict erosion wear.

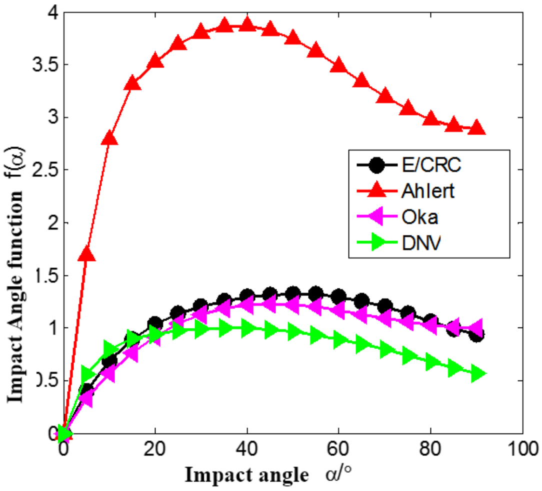

Figure 5 Impact function of different erosion models

In order to choose the most suitable prediction model among DNV model, E/CRC model and Oka model, CFD simulation analysis of the erosion in flexible tubes based on these three models are conducted, and simulation results are compared with the experimental results of Helgaker (Helgaker *et al*. 2017). The difference between the initial calculation parameters is that the selected erosion model is different, that is, the mechanical behavior of particles after collision with the wall is different. In addition, other parameters such as inlet and outlet boundary conditions, particle mass flow, etc. remain consistent. Table 5 shows the simulation conversion results under 11 different working conditions and three different erosion models. The comparison between different calculation results is the maximum erosion depth EW.

It is difficult to tell which of the three erosion prediction models is the best choice based on data provided in the above table. The experimental results are hence compared with the simulation results of the three models in Figure 6. The abscissa represents the experimental result (mm/ton), and the ordinate represents the simulation result (mm/ton). The closer the data point is to the straight line $y = x$, the more accurate the erosion prediction model is. In addition, error bands are given above and below $y = x$. and almost all Oka data points fall within the error band near $y = x$, indicating that the Oka model results are close to the experimental results, and the predicted results have less error than the other results. Because the Oka model takes into account the accumulation of plastic deformation effect of materials and the microcutting effect of particles on materials, the effects of particle impact angle, velocity, particle size and material hardness are fully considered in the model (Peng and Cao, 2016).

Table 5 Erosion experiment result and numerical simulation result of flexible bend pipe

Working condition	**Particle velocity (m/s)**	**experiment value (mm/ton)**	**DNV (mm/ton)**	**E/CRC(mm/ton)**	**Oka(mm/ton)**
1	47	0.077	0.057	0.067	0.08
2	36	0.032	0.027	0.037	0.029
3	30	0.022	0.012	0.029	0.02
4	30	0.024	0.017	0.027	0.026
5	30	0.023	0.017	0.03	0.028
6	35	0.031	0.026	0.016	0.028
7	35	0.037	0.026	0.046	0.030
8	35	0.036	0.045	0.026	0.030
9	40	0.050	0.054	0.066	0.042
10	40	0.053	0.067	0.046	0.06
11	40	0.056	0.036	0.068	0.062

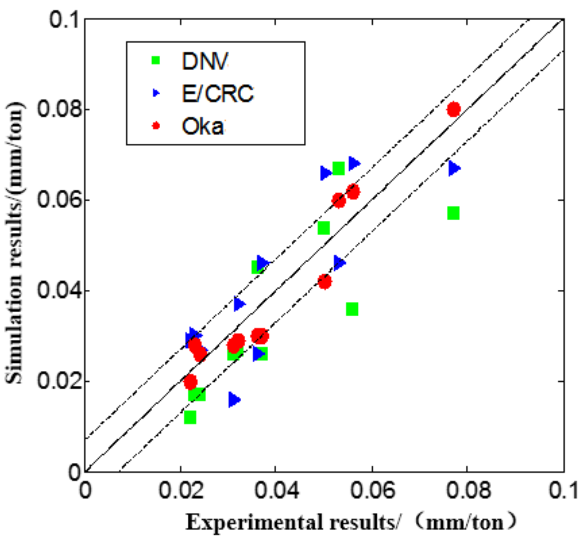

Figure 6 Erosion comparison of three erosion prediction models with experiment results

The erosion simulation diagrams using three different models to simulate case 1 are shown in Figure 7. It can be seen from the simulation that the result of the Oka model is 6.10e-5 kg/m^2•s (*ED* = 7.8e-6 mm/s, *EW* = 0.0776 mm/ton), the result of the DNV model is 2.92e-5 kg/m^2•s (*ED* = 3.7e-6 mm/s, *EW* = 0.0372mm/ton), and the result of the E/CRC model is 5.92e-5 kg/m^2•s (*ED* = 7.5e-6 mm/s, *EW* = 0.0753 mm/ton). It can be seen that the Oka model is the closest to the experimental results (*EW* = 0.077 mm/ton, *ER* = 6.0522e-5 kg/m^2•s). Therefore, this paper uses the Oka model to predict and analyze the erosion of flexible pipes.

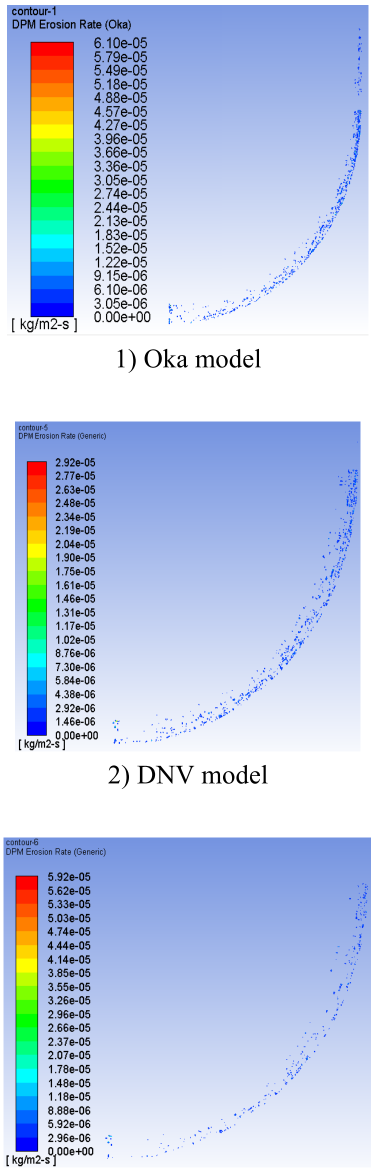

1) Oka model

2) DNV model

3) E/CRC model

Figure 7 Erosion contour of three erosion prediction model.

4.2 ANALYSIS OF INTERNAL FLOW FIELD LAW

4.2 (a) Velocity Analysis of Flow Field

The velocity distribution of the fluid in the flexible pipe is shown in Figure 8 and the velocity contours on the 7 sections of the curved part from 0 ° to 90 ° are given.

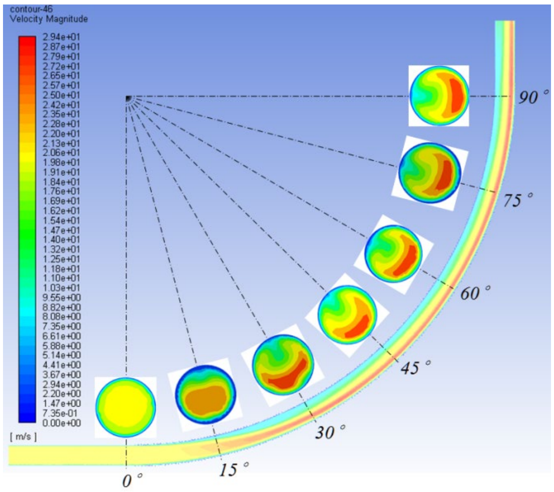

Figure 8 Velocity distribution contour of flexible bend pipe

From the perspective of the overall velocity distribution of the flexible pipe, the velocity in the straight pipe segment at the inlet is basically constant, and the parts with higher velocity are basically distributed at the center of the pipe. In the bending section, the maximum velocity is not located on the center line of the pipe, but on the lower part of the center line. This is because the fluid is forced to move to the position near the outer wall under the action of centrifugal force. Figure 9 shows the distribution of velocities at 7 positions of 0°~90° along the curvature angle on the central section (the length of the x-coordinate is the diameter of the flexible bending pipe). At 0°, the velocity in most areas of the section remains about 20 m/s, and at 15°, the velocity in most areas of the section remains about 26 m/s. The changing rule of the distance along the central angle of the velocity at other positions is that the velocity increases first and then decreases. The decrease of the velocity near the outer wall is due to the increase of the fluid viscosity at the outer wall, resulting in the velocity at the outer wall being less than the velocity away from the wall surface.

4.2 (b) Analysis of Flow Field Pressure

The pressure distribution of the fluid on the inner central section of the flexible pipe decreases from the inlet to the outlet (see Figure 10). However, the pressure on the outer side of the bent part of the flexible pipe is higher and the pressure on the inner side is lower, which is mainly due to the centrifugal force generated when the fluid flows through the bent part, thus causing greater extrusion on the outer side of the bent pipe. At the same time, when the sand-carrying gas enters the curved part of the flexible pipe, the flow state is hindered by the outer wall surface. Due to the compressibility of the gas, the gas is compressed after the flow is blocked, which can also cause the external pressure to rise.

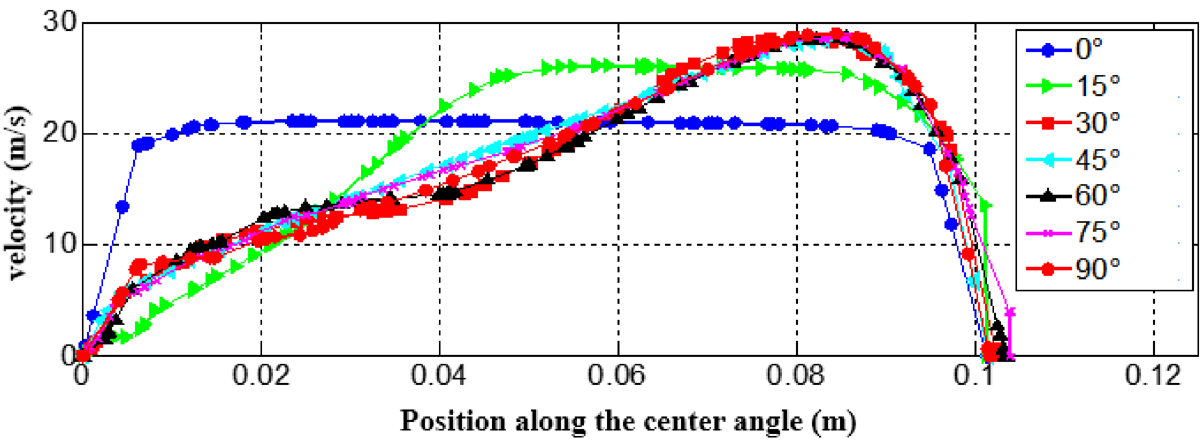

Figure 9 Distribution of velocity at 7 different positions along the core angle of flexible bend pipe

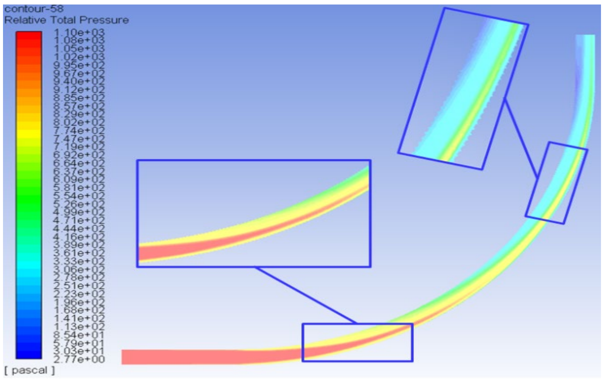

Figure 10 Pressure distribution contour of flexible bend pipe

Figure 11 shows the distribution of the pressure at 6 positions in 15°~90° at different angles along the curvature of the curved section on the central section (the length of the abscissa is the diameter of the curved flexible pipe). It can be seen that the change law of the distance of the pressure at the six positions is first increased and then decreased. In the distribution of pressure at different angular positions, because 15° is closer to the inlet section, the flow is more stable while the pressure in the middle area remains at a certain value. The other angles all reach the peak at 4/5 along the direction of the central angle. As the angle increases, the maximum pressure decreases continuously, indicating that the pressure decreases continuously when the fluid is transported in a curved flexible pipe.

4.2 (c) Erosion Distribution of Flow Field

The erosion contour of the flexible pipe is shown in Figure 12. The outer part of the picture is the overall erosion cloud diagram of the flexible pipe, while the inner part is the cloud diagram of the erosion part. The two local magnification images of the inner part are the erosion effect diagrams of the 20°~30° and 70°~80° parts of the flexible pipe.

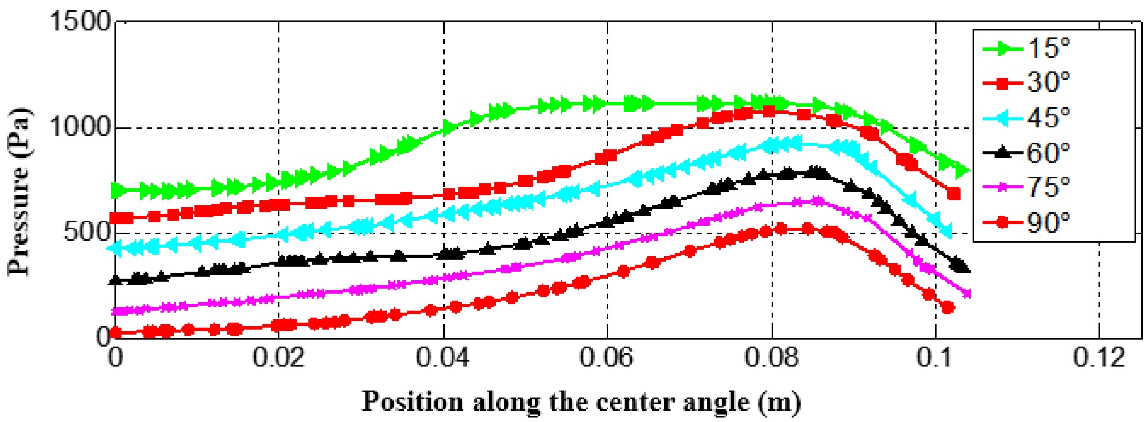

Figure 11 Distribution of pressure at 6 different positions along the core angle of flexible bend pipe

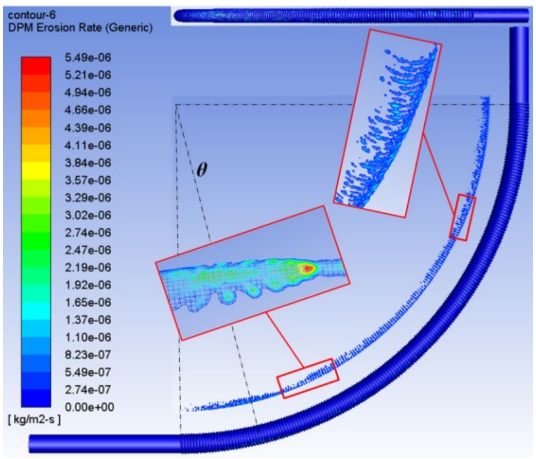

Figure 12 Erosion contour of flexible pipe

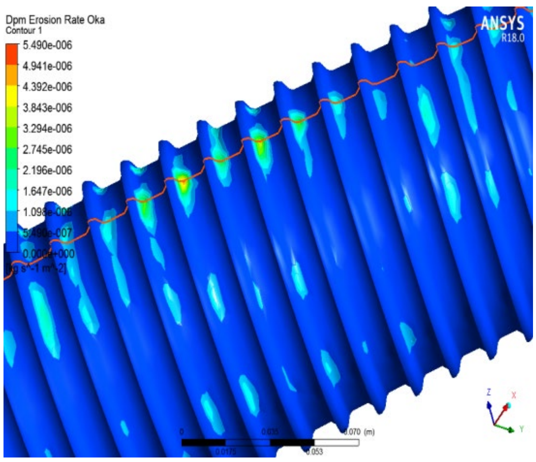

Figure 13 Local contour of flexible pipe

From the perspective of maximum erosion, it can be found that the maximum erosion locations are distributed between 20°~30°, which is consistent with the actual measurement results of the experiment (Helgaker *et al.* 2017). The larger erosion areas on the outer tube wall of the flexible pipe are distributed at the intersection of the outer wall surface of the flexible pipe and the center plane, and basically occur at the arc connecting the arch back and the straight section. There is almost no erosion occurs in the groove. It is consistent with the actual situation and proves the correctness of the simplified model established in Section 3.2. From the perspective of overall erosion, the maximum erosion rate is 5.49×10^{-6} kg/m^2•s.

4.3 PARAMETRIC STUDIES

4.3.1 Effects of Particle Parameters

Figures 14-15 illustrate the effects of particle velocity, particle diameter and particle mass flow rate on the maximum erosion rate of flexible pipes. The erosion rate changes of the flexible pipe are analyzed respectively under particle velocities of 5 m/s, 10 m/s, 15 m/s, 20 m/s and 25 m/s with particle diameters being 50 μm, 100 μm, 150 μm and 200 μm, and particle mass flow rates being 0.005 kg/s, 0.01 kg/s, 0.015 kg/s, 0.02 kg/s, 0.025 kg/s and 0.030 kg/s, respectively.

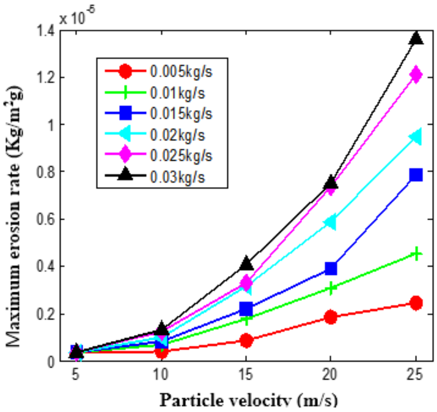

a) Particle diameter 100μm

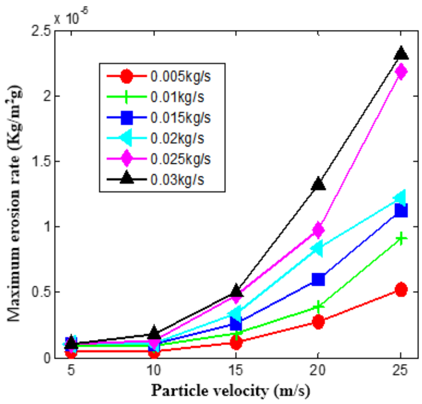

b) Particle diameter 150μm

Figure 14 Maximum erosion rate of flexible pipes at different particle diameters

It is clear that the maximum erosion rate increases exponentially with the increase of particle velocity. It is mainly because the higher the velocity is, the more kinetic energy can be converted into the specific pressure energy on the pipe wall, and the greater the shear stress of the pipe wall can be generated (Banakermani *et al.*, 2018). Therefore, particle velocity has a greater impact on the erosion.

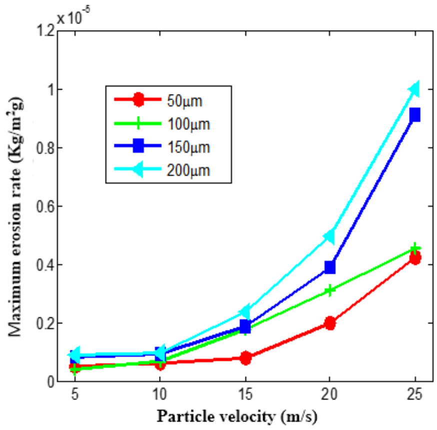

a) Particle mass flow 0.01kg/s

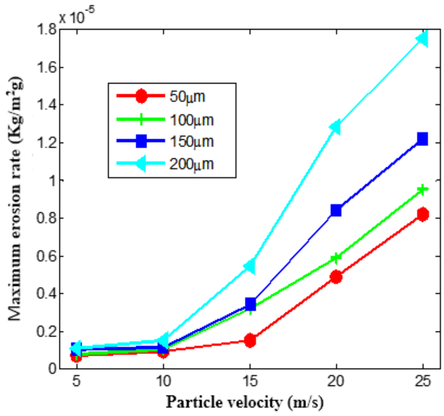

b) Particle mass flow 0.02kg/s

Figure 15 Maximum erosion rate of flexible pipes at different particle mass flow

In addition, the erosion rate increases with the increase of the particle diameter, mainly because the inertial force dominates when the particle diameter increases. The larger the particle, the greater the inertial force, and the greater the erosion rate caused by the collision of the particle with the pipe wall.

Figures 16-17 show the relationship between the maximum erosion rate of curved flexible pipes and particle velocity, particle diameter and particle mass flow rate. The erosion changes of flexible pipe are analyzed under the particle mass flow rate of 0.005 kg/s, 0.01 kg/s, 0.015 kg/s, 0.02 kg/s, 0.025 kg/s, 0.03 kg/s with particle velocity being 10 m/s, 15 m/s, and the particle diameter being 50 μm, 100 μm, 150 μm, 200 μm.

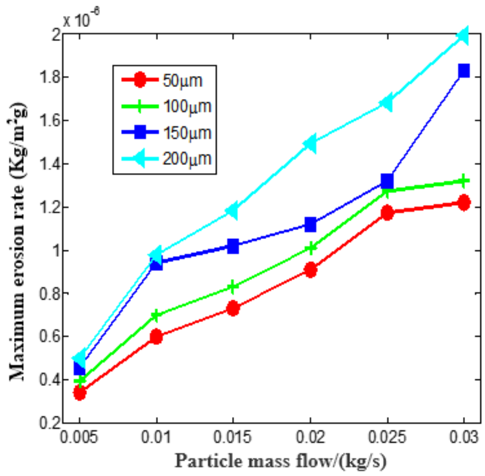

a) Particle velocity 10 m/s

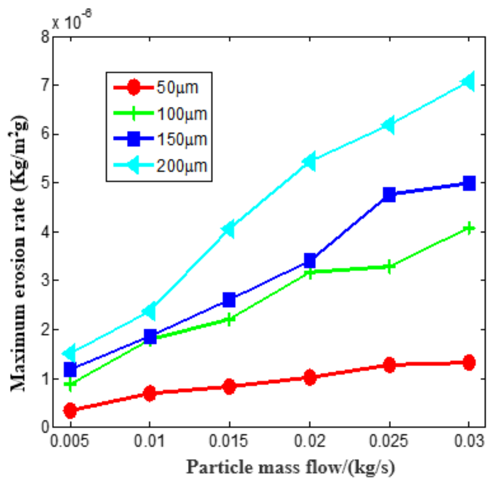

b) Particle velocity 15 m/s

Figure 16 Maximum erosion rate of flexible pipe at different particle speeds

Further, as shown in Figures 16-17, the erosion rate increases with the increase of the particle mass flow rate, mainly because the number of particles impacting the wall surface increases with the increase of the particle mass flow rate, and the number of particles impacted per unit area increases (Cao *et al*., 2016).

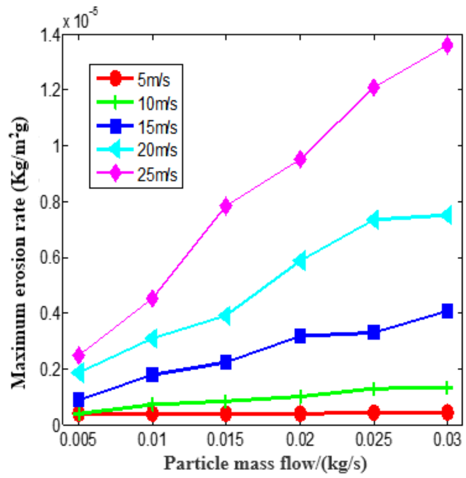

a) Particle diameter 100 μ

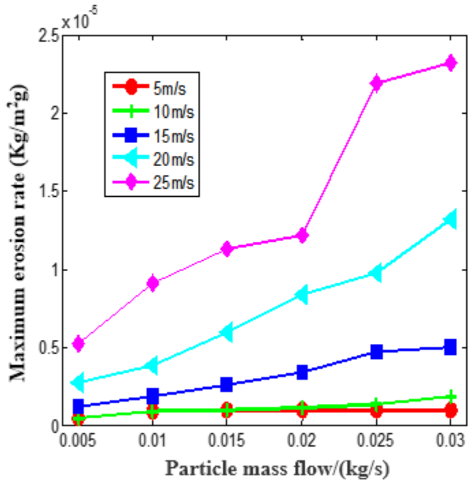

b) Particle diameter 150 μm

Figure 17 Maximum erosion rate of flexible pipes at different particle diameters

Through the above parametric analysis, it is found that the erosion rate of the flexible pipe changes exponentially with respect to the particle velocity and linearly with respect to the mass flow of the particles. The exponential function and the polynomial can be used to fit separately. The fitting formula is:

$$er(v_p, m_p) = \sum_{i=0}^{M} a_i \, v_p^i + \sum_{j=1}^{N} b_j \, m_p^j + \sum_{i=1}^{M}\sum_{j=1}^{N} c_{ij} \, v_p^i m_p^j \quad (M \le 3, N \le 2) \tag{28}$$

where, *er* represents the erosion rate of the flexible pipe, kg/m^{2}s; v_p represents the particle velocity, m/s; m_p represents the particle mass flow rate, kg/s.

The tool box cftool for data fitting in Matlab is used to conduct three-dimensional interpolation for the erosion rate of flexible pipe with pipe diameter of 4 in. and pipe curvature radius of 72 in., and different fitting precision is obtained by changing the number of terms *M* and *N*. When *M* = 3 and *N* = 2, *r*-square greater than 0.99 has a good fitting effect. At the same time, it is found that the erosion rate data points of the flexible pipe are well distributed on the fitting surface of the erosion rate about particle velocity and particle mass flow.

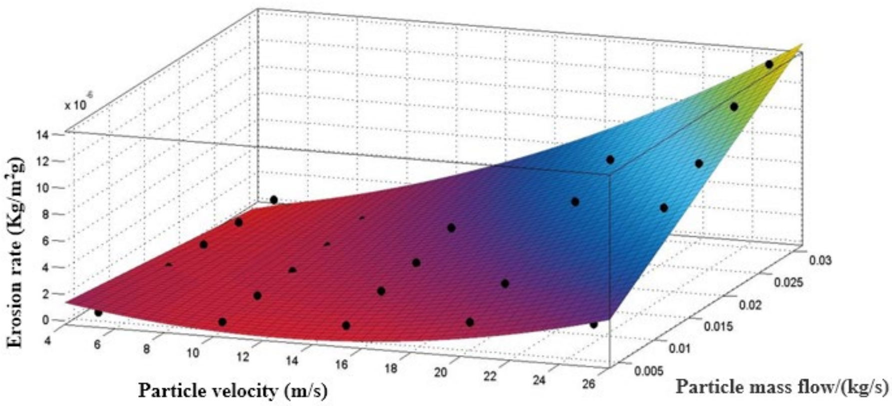

Figure 18 Fitting surface of particle velocity and particle mass flow rate about flexible bend pipe erosion rate (*dp* = 100 μm)

Table 6 Formula coefficient

	a_0	a_1	a_2	a_3	b_1	b_2	c_{11}	c_{12}	c_{21}
100 μm	5.981e-7	-5.107e-8	2.068e-9	-6.467e-11	-1.367e-5	1.290e-3	-4.191e-6	-1.910e-4	1.108e-6
150 μm	-8.524e-7	1.672e-7	-5.804e-9	2.163e-10	3.205e-4	-4.843e-3	-5.293e-5	5.838e-4	2.248e-6

4.3.2 Effects of Carcass Structural Parameters

The relationship between the maximum erosion rate of the flexible pipe and the diameter of the pipe under different curvature radius are shown in Figure 19. The erosion changes of the flexible pipe are analyzed when the particle velocity is 10m/s, the particle mass flow rate is 0.005 kg/s, the diameter of the pipe is 100 μm, the diameter of the pipe is 2 in, 4 in, 6 in, 8 in, and the radius of curvature is 22, 24, 26, and 28.

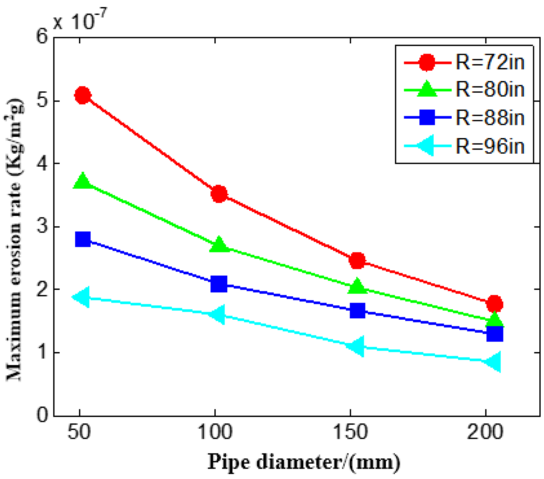

Figure 19 Erosion rate under different pipe diameters and bend curvature radius

As it can be seen from Figure 19, the erosion rate decreases with the increase of the pipe diameter, mainly because the large diameter flexible pipe has a larger inner wall area, and the number of particle collisions per unit area decreases. The erosion rate decreases with the increase of the curvature radius of the pipe, mainly because with the increase of the curvature radius of the pipe, the flexural to diameter ratio of the flexible pipe increases, the flow in the pipe tends to be smooth, and the impact of particles on the pipe wall weakens, so the erosion rate decreases (Zhang *et al.*, 2016).

The erosion rate of the flexible pipe can be fitted with a polynomial about the diameter of the pipe and the radius of curvature of the pipe. The fitting formula is:

$$er(D,R) = \sum_{i=0}^{M} a_i\, D^i + \sum_{j=1}^{N} b_j\, R^j + \sum_{i=1}^{M}\sum_{j=1}^{N} c_{ij}\, D^i R^j \quad (M \le 2, N \le 2) \tag{29}$$

where，*er* represents the erosion rate of the flexible pipe (kg/m^2•s), *D* represents the diameter of the pipe (in); *R* represents the radius of curvature of the pipe (in).

When $M = 2$ and $N = 2$, r-square is 0.9912, indicating high fitting accuracy. At this time, the erosion rate data points of the flexible pipe are well distributed on the fitting surface of the erosion rate about the pipe diameter and the pipe curvature radius.

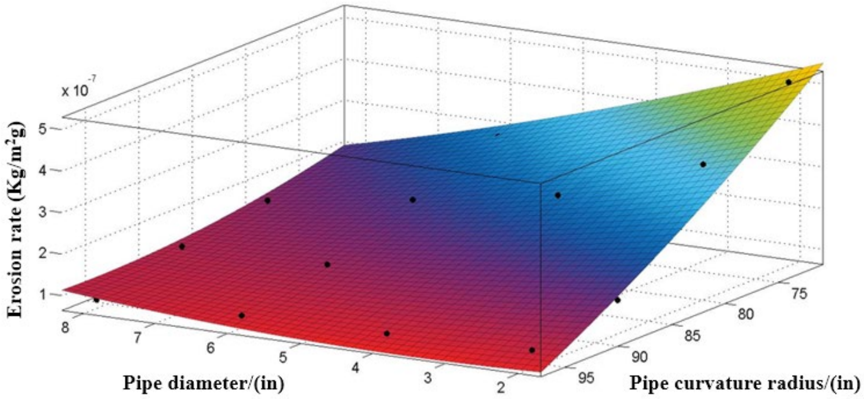

Figure 20 Fitting surface of pipe diameter and pipe curvature radius about flexible pipe erosion rate

Table 7 Formula coefficient

Coefficient	a_0	a_1	a_2	a_3	a_4	a_5
Value	3.212e-6	-2.333e-7	1.859e-9	-4.623e-8	1.453e-10	2.269e-6

5. CONCLUSION

There are only a limited number of studies and experiments for complex flexible pipes, which is insufficient to guide production operations. In this paper, the optimal erosion prediction model of flexible pipe is established, the sensitivity analysis of multi-parameters is compared, and the formulas of erosion rate of curved flexible pipe with different parameters are fitted. The main conclusions are as follows:

(1) A simplified physical erosion model of carcass layer of flexible pipe is established, grid-independent analysis and length analysis of inlet and outlet straight pipe are carried out, and determine the use of the 4 mm grid size and 4*D*/8*D* length of inlet and outlet straight pipe.

(2) The applicability analysis is carried out for different erosion prediction models, and the Oka model is selected for simulation analysis by comparing with the existing erosion experimental data of flexible curved tubes. Based on the Oka erosion model, sensitivity effects of fluid parameters such as particle velocity, particle diameter, and particle mass flow, and structural parameters such as pipe diameter and pipe curvature radius on the erosion rate of the flexible pipes are analyzed. It is found that the maximum erosion rate of flexible pipes increase with the increase of particle velocity, particle diameter, and particle mass flow, which increased exponentially with the increase of particle velocity. The maximum erosion rate of flexible pipes decreases with the increase of pipe diameter and pipe curvature radius.

(3) The particle parameters such as particle velocity, particle mass flow rate, particle diameter and other pipe structure parameters such as pipe diameter and pipe curvature radius are numerically fitted. The quantitative description of erosion rate of curved flexible pipe with respect to particle parameters and pipe structure parameters is given, which provides an important reference basis for the control of particle parameters and the design of curved flexible pipe in engineering practice.

6. ACKNOWLEDGMENTS

The work was supported by the National Key Research and Development Plan (Grant no. 2016YFC0303704), National Natural Science Foundation of China (Grant no. 51879271), the 111 Project (B18054).

7. REFERENCES

1. AHLERT, K. R. (1994) *Effects of particle impingement angle and surface wetting on solid particle erosion of aisi 1018 steel*. Ph.D. thesis, Department of Mechanical Engineering, The University of Tulsa.
2. ARABNEJAD, H., MANSOURI, H., SHIRAZI, S. A., *et al*. (2015) *Development of mechanistic erosion equation for solid particles*. Wear, 332-333.
3. BANAKERMANI, M. R., NADERAN, H. and SAFFAR-AVVAL, M. (2018) *An investigation of erosion prediction for 15° to 90° elbows by numerical simulation of gas-solid flow*. Powder Technology, 334: 9-26.
4. CAO, X., XU, K. and WEN, W. (2016) *Simulation and Analysis of Liquid-Solid Two-*

phase Flow Erosion Failure in Pipe Bends. Surface Technology, 124-131.

5. CHEN, X., MCLAURY, B. S. and SHIRAZI S. A. (2004) *Application and experimental validation of a computational fluid dynamics (CFD)-based erosion prediction model in elbows and plugged tees*. Computers and Fluids, 33(10): 1251-1272.
6. CHONG, Y. W., CHRISTOPHER, B. S. L. and HENRI M. (2015) *Flexible pipe erosion modeling*. Proceeding of the 11th International Conference on CFD in the Minerals and Process Industries CSIRO, Melbourne, Australia.
7. DET NORSKE VERTITAS. (2007) *Recommended Practice RP 0501: Erosive Wear in Piping Systems*. 2007.
8. FINNIE, I. (1958) *The mechanism of erosion of ductile metals*. Proceedings of 3rd US National Congress of Applied Mechanics, 527-532.
9. GRANT, G. and TABAKOFF, W. (1973) *An experimental investigation of the erosion characteristics of 2024 aluminum alloy*. Cincinnati: Department of Aerospace Engineering, University of Cincinnati, Report 73-37.
10. HELGAKER, J. F., IJZERMANS, S., LANDHEIM, T. J., *et al*. (2017) *Large-scale erosion testing of an unbonded flexible pipe*. SPE Journal, 22(3): 1-10.
11. KVERNVOLD, O. and NOKLEBERG L. (1989) *FPS2000/Flexible pipes-Erosion in flexible pipes*. Veritec Report No. 89-3303.
12. KVERNVOLD, O, SANDBERG, R and RONOLD, A. (1990) *Experimental investigation of the erosion characteristics of the steel carcass in COFLEXIP flexible pipes. 2" rough bore flexible pipe, gas phase only*. Veritec Report No. 90-3691.
13. LI, X., JIANG, X. L. and HOPMAN, H. (2018) *A strain energy-based equivalent layer method for the prediction of critical collapse pressure of flexible risers*. Ocean Engineering, 164: 248-255.
14. MORSI, S. A. and ALEXANDER, A. J. (1972) *An investigation of particle trajectories in two-phase flow systems*. Journal of Fluid Mechanics Digital Archive, 55(02): 193-208.
15. ØSTERGAARD, N. H., LYCKEGAARD, A. and ANDREASEN J. H. (2012) *On modelling of lateral buckling failure in flexible pipe tensile armour layers*. Marine Structures, 27(1): 64-81.
16. OKA, Y. I., OKAMURA, K. and YOSHIDA, T. (2005) *Practical estimation of erosion damage caused by solid particle impact. Part 1: Effects of impact parameters on a predictive equation*. Wear, 1-6(259): 95-101.
17. OKA, Y. I. and YOSHIDA T. (2005) *Practical estimation of erosion damage caused by solid particle impact. Part 2: Mechanical properties of materials directly associated with erosion damage*. Wear, 1-6(259): 102-109.
18. PARSI, M., KARA, M., AGRAWAL, M., *et al*. (2017) *CFD simulation of sand particle erosion under multiphase flow conditions*. Wear, 376–377:1176-1184.
19. PARSI, M., AL-SARKHI, A., KARA M., *et al*. (2017) *A new dimensionless number for solid particle erosion in natural gas elbows*. Wear, 390-391: 80-83.
20. PARSI, M., NAJMI, K., NAJAFIFARD, F., *et al*. (2014) *A comprehensive review of solid particle erosion modeling for oil and gas wells and pipelines applications*. Journal of Natural Gas Science and Engineering, 21: 850-873.
21. PENG, W. and CAO, X. (2016) *Influence of Pipe Parameters on Flow Field of Liquid-solid Two-phase Flow and Erosion of Pipe Bend*. Journal of Chinese Society for Corrosion and Protection, 1: 87-96
22. PSA-NORWAY. (2007) *Flexible Pipes. Failure Modes, Inspection, Testing and Monitoring*. Report P5996-RPT01-Rev02.
23. ZAMANI, M., SEDDIGHI, S. and NAZIF, H. R. (2017) *Erosion of natural gas elbows due to rotating particles in turbulent gas-solid flow*. Journal of Natural Gas Science and Engineering, 40: 91-113.
24. TANG, M. G., LU, Q. Z., YAN, J., *et al*. (2016) *Buckling collapse study for the carcass layer of flexible pipes using a strain energy equivalence method*. Ocean Engineering, 111: 209-217.
25. VERSTEEG H K, MALALASEKERA W. An introduction to computational fluid dynamics: the finite volume method[M]. Pearson education, 2007.
26. WANG, K., LI, X. F., WANG, Y. S., *et al*. (2016) *Numerical investigation of the erosion behavior in elbows of petroleum pipelines*. Powder technology, 314: 490-499.

27 ZHANG, Y., REUTERFORS, E. P., MCLAURY, B.S., *et al*. (2007) *Comparison of computed and measured particle velocities and erosion in water and air flows*. Wear, 1(263): 330-338.

28. ZHANG, J., KANG, J., FAN, J., *et al*. (2016) *Study on erosion wear of fracturing pipeline under the action of multiphase flow in oil & gas industry*. Journal of Natural Gas Science and Engineering, 32: 334-346.